Article Type:	Invited Methods Collection - JoVE Produced Video
Manuscript Number:	JoVE62724R2
Full Title:	Quantitative MRI of Endothelial Permeability and (Dys)function in Atherosclerosis
Corresponding Author:	Alkystis Phinikaridou King's College London UNITED KINGDOM
Corresponding Author's Institution:	King's College London
Corresponding Author E-Mail:	alkystis.1.phinikaridou@kcl.ac.uk
Order of Authors:	Begoña Lavin
	Marcelo Andia
	Prakash Saha
	René Botnar
	Alkystis Phinikaridou
Additional Information:	
Question	**Response**
Please specify the section of the submitted manuscript.	Bioengineering
Please indicate whether this article will be Standard Access or Open Access.	Open Access ($3900)
Please indicate the **city, state/province, and country** where this article will be **filmed**. Please do not use abbreviations.	London, UK
Please confirm that you have read and agree to the terms and conditions of the author license agreement that applies below:	I agree to the UK Author License Agreement (for UK authors only)
Please provide any comments to the journal here.	The copyrights document was converted from a pdf to a word file. some formatting issues might occur.

1 **TITLE**:
2 Quantitative MRI of Endothelial Permeability and (Dys)function in Atherosclerosis
3
4 **AUTHORS AND AFFILIATIONS:**
5 Begoña Lavin[1,2,3], Marcelo E. Andia[1,4,5], Prakash Saha[6], René M. Botnar[1,2,7,8], Alkystis
6 Phinikaridou[1,2]
7
8 [1]School of Biomedical Engineering Imaging Sciences, King's College London, London, UK.
9 [2]BHF Centre of Excellence, Cardiovascular Division, King's College London, London, UK.
10 [3]Biochemistry and Molecular Biology Department, School of Chemistry, Complutense University,
11 Madrid, Spain.
12 [4]Radiology Department, School of Medicine, Pontificia Universidad Católica de Chile, Santiago,
13 Chile.
14 [5]ANID - Millennium Science Initiative Program - Millennium Nucleus for Cardiovascular Magnetic
15 Resonance, Santiago, Chile.
16 [6]Academic Department of Vascular Surgery, Cardiovascular Division, King's College London,
17 London, UK.
18 [7]Wellcome Trust and EPSRC Medical Engineering Center, King's College London, UK.
19 [8]Pontificia Universidad Católica de Chile, Escuela de Ingeniería, Santiago, Chile.
20
21 Email Addresses of Co-authors:
22 Begoña Lavin   (blavin@ucm.es)
23 Marcelo E. Andia   (meandia@uc.cl)
24 Prakash Saha   (prakash.saha@kcl.ac.uk)
25 René M. Botnar   (rene.botnar@kcl.ac.uk)
26 Alkystis Phinikaridou (alkystis.1.phinikaridou@kcl.ac.uk)
27
28 Corresponding Author:
29 Alkystis Phinikaridou (alkystis.1.phinikaridou@kcl.ac.uk)
30

31 **KEYWORDS:**
32 endothelial permeability, endothelial dysfunction, MRI, cardiovascular diseases, atherosclerosis,
33 albumin leakage
34

35 **SUMMARY:**
36 We have developed an accurate, non-invasive, and easy-to-use method to quantify endothelial
37 permeability and dysfunction in the arteries using Magnetic Resonance Imaging (MRI), named
38 qMETRIC. This technique enables assessing vascular damage and cardiovascular risk associated
39 with atherosclerosis in preclinical models and humans.
40

41 **ABSTRACT:**
42 Cardiovascular diseases are the leading causes of death worldwide. A permeable/leaky and
43 dysfunctional endothelium is considered the earliest marker of vascular damage and thought to
44 drive atherosclerosis. A method to identify these changes *in vivo* would be desirable in the clinic.

45 Magnetic resonance imaging (MRI)-based tools and other technologies have enabled a profound
46 understanding of the role of the endothelium in cardiovascular diseases and risk *in vivo*. There is,
47 however, a need for reproducible and simple approaches for extracting quantifiable data
48 reflective of endothelial damage from a single imaging study. A non-invasive, easy-to-implement,
49 and quantitative MRI workflow was developed to acquire and analyze images that allow the
50 quantification of two imaging biomarkers of arterial endothelial damage (leakiness/permeability
51 and dysfunction). Here, the protocol describes the application of this method in the
52 brachiocephalic artery of atherosclerotic ApoE^{-/-} mice using a clinical MRI scanner. First, late
53 gadolinium enhancement (LGE) and Modified Look-Locker Inversion Recovery (MOLLI) T1
54 mapping protocols to quantify endothelial leakage using an albumin-binding probe are described.
55 Second, anatomic, and quantitative blood flow sequences to measure endothelial dysfunction,
56 in response to acetylcholine are described. Importantly, the method outlined here allows the
57 acquisition of high-spatial-resolution 3D images with large volumetric coverage enabling accurate
58 segmentation of vessel wall structures to improve inter- and intra-observer variability and to
59 increase reliability and reproducibility. Additionally, it provides quantitative data without the
60 need for high-temporal resolution for complex kinetic modeling, making it model-independent
61 and even allowing for imaging of highly mobile vessels (coronary arteries). Therefore, the
62 approach simplifies and expedites data analysis. Finally, this method can be implemented on
63 different scanners, can be extended to image different arterial beds, and is clinically applicable
64 for use in humans. This method could be used to diagnose and treat patients with atherosclerosis
65 by adopting a precision-medicine approach.
66
67 **INTRODUCTION:**
68 Cardiovascular diseases (CVDs) remain the leading cause of mortality and morbidity worldwide,
69 accounting for nearly one-third of deaths[1], and the cause of lifelong disabilities that exert a high
70 financial cost on the healthcare systems[1]. Among CVDs, ischaemic heart disease and stroke are
71 primarily caused by atherosclerotic plaques. Atherosclerosis is a multifactorial disease; however,
72 a common hallmark is early damage of the vascular endothelial cells that lead to the formation,
73 progression, and eventual complications of atherosclerosis. An intact vascular endothelium has
74 fundamental vasculo-protective properties[2]. The endothelium regulates vascular permeability by
75 controlling translocation of cells and molecules between the systemic circulation and the vessel
76 wall; controls vascular tone by balancing the production of vasodilators (e.g., nitric oxide,
77 prostacyclin) and vasoconstrictors (e.g., endothelin-1, angiotensin II); and also has anti-coagulant
78 properties. However, both the function and permeability of the endothelial cells can deteriorate
79 in the presence of cardiovascular risk factors (e.g., smoking, high cholesterol, diabetes, systemic
80 inflammation, oxidative stress) and by blood flow hemodynamic patterns. A dysfunctional
81 endothelium has reduced vasodilation in response to stressors, consequently increasing arterial
82 stiffness. In addition, a permeable/leaky endothelium has widened tight gap junctions between
83 adjacent cells[3–7]. Such change occurs both on the luminal endothelium and newly-formed plaque
84 microvessels that appear fragile, leaky, and dysmorphic[8]. Permeable endothelial cells act as entry
85 points for plasma-borne molecules and cells—exacerbating the risk of cardiovascular disease.
86
87 Building on this knowledge, in the past 15 years, endothelial permeability and function has
88 emerged as a promising imaging and therapeutic target to better diagnose subjects at risk for

89 cardiovascular disease and to assess the effects of known or novel drugs. However, direct and
90 quantitative imaging of endothelium function is limited[9–12]. Currently, much of the interpretation
91 of endothelial function *in vivo* is based on studies of endothelial-dependent dilation (FMD) in
92 peripheral vessels whose function modestly correlates with atherosclerosis burden in vascular
93 beds that cause clinical events[13–15]. Only a limited number of imaging studies have shown a direct
94 link between endothelial dysfunction and atherosclerosis burden *in vivo*[9–12]. Conversely, more
95 accessible MRI-based approaches have enabled imaging endothelial permeability more widely.
96 Using the percent vessel wall signal enhancement after administration of MRI gadolinium agents
97 has provided a semi-quantitative measurement of endothelial permeability[16,17]. Later, the
98 development of dynamic contrast-enhanced (DCE) protocols has permitted an improved and
99 more quantitative measurement of vascular endothelial permeability. Quantitative parameters
100 such as the contrast extravasation rate (K^{trans}) and microvascular volume ($V\rho$) derived from
101 kinetic modeling or the area under the curve (AUC), upslope, time to peak, and peak
102 concentration extracted from non-modeled methods correlated not only with endothelial
103 permeability but also plaque vascularity[18–20]. However, the application of vascular DCE remains
104 challenging despite significant technical advances because: (i) it requires both high spatial (0.5–
105 0.7 mm^2) and temporal resolution[21] for accurate delineation of the vessel wall. Sampling the
106 concentration of contrast agent in the blood to calculate the arterial input function also requires
107 kinetic modeling, which leads to a trade-off of either limiting anatomical coverage[22,23] to gain
108 temporal resolution or vice versa[24,25]; (ii) data analysis may require complex pharmacokinetic
109 modeling (e.g., Patlak vs. Tofts); (iii) provides limited image quality, poor scan-rescan
110 reproducibility, and average inter-observer and intra-observer variability[26,27]. Therefore, there is
111 still a need for reproducible and simple approaches for extracting direct and quantifiable data of
112 endothelial permeability and (dys)function from single imaging studies that could have better
113 clinical utility.
114
115 Here, we have developed a non-invasive, easy-to-implement, and quantitative MRI to acquire
116 and analyze images that allows direct quantification of two markers of arterial endothelial
117 damage (leakiness/permeability and dysfunction) using preclinical models of atherosclerosis in a
118 single scan. The method is named Quantitative MRI of EndoThelial peRmeabIlity and dysfunCtion
119 (**qMETRIC**). It involves the acquisition of late gadolinium enhancement (LGE) and Modified Look-
120 Locker Inversion Recovery (MOLLI) T1 mapping protocols to quantify endothelial leakage, after
121 administration of an intravascular albumin-binding probe; and acquisition of anatomic and
122 quantitative blood flow sequences to measure endothelial dysfunction, in response to an
123 acetylcholine bolus. We have demonstrated that qMETRIC accurately detects: the severity of
124 atherosclerosis and the risk of complications; treatment responses; and can be adapted for use
125 in patients[5–7]. Importantly, the method outlined here allows the acquisition of high-spatial-
126 resolution images to enable accurate segmentation of the vessel wall to minimize inter/intra-
127 observer bias and to increase reliability and reproducibility with large anatomical coverage.
128 Finally, this method can be adapted for use on different scanners and can be extended to image
129 different arterial beds (even coronary arteries[28]). The straightforward workflow makes this
130 approach more accessible to the cardiovascular imaging community.
131
132 **PROTOCOL:**

All components of this study were carried out in accordance with the UK Animals (Scientific Procedures) Act, 1986, and with the approval of King's College London Ethical Review Panel. The experimental workflow is summarized in **Figure 1**.

1.   Animal preparation

1.1.   Induce atherosclerosis by feeding ApoE$^{-/-}$ mice a high-fat diet containing 21% fat from lard and 0.15% (wt/wt) cholesterol on average for up to 12 weeks.

1.2.   Load a 29 G needle insulin syringe with the right volume of the contrast agent (gadofosveset trisordium) to achieve a dose of 0.03 mmol/kg. Keep the injection volume between 50–150 μL.

1.3.   Place the cage on a heating pad set to 37 °C to pre-heat the animal and maintain the body temperature.

1.4.   Induce anesthesia by placing the mouse in an induction box lined with absorbent tissues. Adjust the flowmeter to 3%–5% of isoflurane at 1 L/min of O_2 for about 3–5 min.

NOTE: Ensure correct anesthesia depth by identifying the slowing breath rate, which should decrease to less than 70 breaths per minute (bpm).

1.5.   Confirm anesthesia using the toe pinch method (i.e., loss of withdrawal reflex to toe pinch). Transfer the animal to a holder and insert its nose into a nose cone. Place the holder on a heating pad to maintain the animals' body temperature.

1.6.   Maintain anesthesia, delivered through the nose, by setting the anesthesia airflow in the holder to 1%–2% isoflurane at 1 L/min of O_2.

1.7.   Apply vet ointment on the animal's eyes to prevent dryness while under anesthesia.

1.8.   Place the animal either prone or on its side and clean the tail with an alcohol swab. Locate one of the two tail veins. If necessary, warm up the tail with a UV lamp to make the tail veins more visible.

1.9.   Insert the 29 G insulin needle parallel to the vein with the bevel of the needle facing up. Gently inject the volume of the prefilled syringe containing gadofosveset trisodium. Ensure that there is no bleeding at the injection site after withdrawing the needle.

1.10.   Wait for 30 s for gadofosveset to circulate, and then transfer the mouse to the MRI bed.

2.   Preparation of the MRI scanner (see Figure 1)

2.1.   Cover the MRI table with absorbent tissues.

177

178   2.2.   Place the MRI single-loop receiver coil on the MRI bed. Use a platform to raise the receiver
179   coil and avoid direct contact between the receiver coil and the MRI table.

180

181   2.3.   Secure the coil to the platform using surgical tape.

182

183   2.4.   Place and secure the tubing connected to a circulating heating pump around the coil and
184   set it to 37 °C to maintain the animal's body temperature during imaging.

185

186   2.5.   Place the anesthesia delivery tubing into the bore of the MRI scanner and tape it so that
187   the nose cone reaches the tip of the receiver coil where the animal's head will be placed.

188

189   2.6.   Turn on the in-bore camera to monitor the animal from the console room.

190

191   2.7.   In the MRI console room, use the software interface to start a new study for the animal
192   (patient).

193

194   **3.   Animal positioning in the MRI scanner and monitoring (see Figure 2)**

195

196   3.1.   Transfer the anesthetized animal to the scanner room. Place the mouse in the prone
197   position on the receiver coil and ensure that its snout fits into the nose cone to maintain
198   anesthesia. Turn the anesthesia airflow to 1%–1.5% isoflurane at 1 L/min of O_2.

199

200   3.2.   Ensure to place the animal on the MRI coil with its heart and neck regions located at the
201   center of the receiver coil.

202

203   3.3.   Secure the nose of the mouse into the nose cone, the abdomen, and the tail of the mouse
204   on the platform with tape.

205

206   3.4.   Place four electrodes on the anterior and the rear paws, making sure that the palm of the
207   toes is completely open to record the electrocardiogram (ECG). Use ECG conductive gel on the
208   mouse's paws before attaching the ECG pads to improve conductivity.

209

210   3.5.   Ensure to use tape to firmly attach the electrodes to the platform.

211

212   3.6.   Align the laser of the scanner's bed with the base (proximal end) of the heart; use the
213   clavicle and anterior paw line as a landmark. Position the animal in the magnet's isocenter using
214   an automatic MR table.

215

216   **4.   MRI image planning and acquisition**

217

218   4.1.   Start a scout scan to run the standard calibrations for the MRI system.

219

220   4.2.   Set the monitoring equipment to detect the R-wave of the ECG. Adjust the thresholds for

221 each mouse and within imaging sessions so that there is reliable triggering.
222
223 NOTE: The mouse heart frequency under deep anesthesia usually ranges between 400–600 beats
224 per minute (bpm).
225
226 4.3.   Acquire a 3D gradient echo scan (GRE) to get multiplanar pilot images (scout images) to
227 plan the rest of the scans (see **Table 1** for the MRI acquisition parameters and **Figure 3** for
228 planning).
229
230 4.4.   Identify the heart on the scout images, particularly on the coronal view, most easily by its
231 flow artifacts.
232
233 NOTE: If the images show the mouse is not well centered over the coil or the isocenter, retract
234 the bed and repeat positioning.
235
236 4.5.   Plan a 3D contrast-enhanced MR angiography (MRA) scan (see **Table 1** for scan for the
237 MRI acquisition parameters and **Figure 3** for planning) in a transverse plane extending from the
238 base of the heart toward the neck and carotid arteries with an 8 mm field-of-view (FOV).
239
240 4.6.   Use the maximum intensity projection (MIP) images to visualize the aortic arch,
241 brachiocephalic and carotid arteries and plan the subsequent late gadolinium enhancement
242 (LGE), T1 mapping, and cine scans (see **Figure 3** for representative images).
243
244 NOTE: If the level of the imaging volume is not correct, repeat the acquisition by moving the slices
245 either proximally or distally.
246
247 4.7.   MRI image acquisition to measure endothelial permeability.
248
249 4.7.1.   Use the MIP and transverse MRA images acquired before to plan a single slice 2D-Look-
250 Locker (LL) acquisition perpendicular to the ascending aorta or carotid arteries (see **Table 1** for
251 scan for the MRI acquisition parameters and **Figure 3** for representative images).
252
253 4.7.2.   Set the heart rate to 60 bpm when using a simulated ECG signal or set a blanking period
254 to ensure that the inversion recovery pulse between subsequent inversion recovery pulses is
255 1000 ms when using the recorded ECG signal.
256
257 4.7.3.   Use the Look-Locker images to determine the optimal inversion time (TI) for blood signal
258 nulling required for the LGE scan.
259
260 4.7.4.   LGE imaging: After 20–30 min of injection of gadofosveset, and immediately after the LL
261 scan (described in steps 4.7.1–4.7.3) acquire an LGE scan using an inversion-recovery 3D fast
262 gradient echo sequence (see **Table 1** for the MRI acquisition parameters and **Figure 3** for
263 representative images).
264

265 4.7.5. Plan a transverse 3D fast gradient echo LGE scan to cover the base of the heart (to include
266 part of the aortic root), the brachiocephalic artery (between the aortic root to the subclavian
267 bifurcation), and part of the carotid arteries with an 8 mm field-of-view (FOV) in the foot-head
268 direction using the same geometry as for the MRA above (see **Figure 3** for representative images).

269

270 4.7.6. Set the heart rate to 60 bpm, when using a simulated ECG signal, or set a blank period to
271 ensure that successive inversion recovery pulses occur at every 1000 ms for the LGE scan when
272 using the recorded ECG signal (as for step 4.7.2 above).

273

274 NOTE: This is important for consistent and heart rate independent recovery of the magnetization
275 between successive inversion recovery pulses.

276

277 4.7.7. Insert the T1 obtained from the Look-Locker into the LGE sequence under **Contrast >**
278 **Inversion Delay**.

279

280 4.7.8. T1 mapping imaging: Use a 3D fast gradient echo acquisition to acquire transverse T1
281 mapping images 45 min after injection of gadofosveset. Plan the sequence in the same
282 orientation and geometry as the LGE scan above (see **Table 1** for the MRI acquisition parameters
283 and **Figure 3** for representative images).

284

285 4.7.9. Set the heart rate to 120 bpm, when using a simulated ECG, or set a blanking period to
286 ensure that the inversion recovery pulse between the two imaging trains occurs at every 500 ms
287 when using the recorded ECG trace.

288

289 NOTE: The T1 mapping sequence uses two non-selective inversion pulses with inversion times
290 between 20–2000 ms, followed by eight segmented readouts for eight individual images. The
291 combination of the two imaging trains results in a total of sixteen images per slice with varying
292 inversion times. The images are automatically reconstructed on the scanner using a three-
293 parameter fit model. The equations used to generate the T1 parametric maps are:

294
$$M_z(t) = A - Be^{\frac{-t}{T_1^*}}$$
295

296
$$T_1 = T_1^* \left(\frac{B}{A} - 1\right)$$

297

298 4.8.   MRI image acquisition to measure endothelial function

299

300 4.8.1. Prepare a solution of diluted acetylcholine in saline. Load a 29 G needle insulin syringe
301 with the right volume of solution to achieve (16.6 mg/kg). Keep the injection volume between
302 50–150 µL.

303

304 4.8.2. Using the transverse MRA and corresponding MIP images, place a transverse slice across
305 the brachiocephalic artery, between the aortic root and the subclavian bifurcation (**Figure 3** for
306 representative images).

307

308 4.8.3. Use a transverse 2D gradient echo (GRE) with retrospective ECG gating to acquire
309 temporally-resolved cine images of the brachiocephalic artery (see **Table 1** for the MRI
310 acquisition parameters **Figure 3** for representative images).
311

312 4.8.4. Adjust the number of maximum cardiac phases to the heart rate of each animal.
313

314 NOTE: Typically, 14 cardiac phases provide sufficient temporal resolution.
315

316 4.8.5. After acquiring the baseline images, enter into the MRI scanner room. While the mouse
317 is anesthetized in the scanner, gently inject acetylcholine intraperitoneally (IP). Avoid moving the
318 mouse on the coil.
319

320 4.8.6. Wait for 6–10 min for the heart rate to stabilize and repeat the acquisition.
321

322 4.8.7. At the end of the imaging procedure, return the mouse to its cage and place the mouse
323 on a heating pad to recover.
324

325 NOTE: Mice are recovered when they regain sufficient consciousness to maintain sternal
326 recumbency.
327

328 4.8.8. Export the acquired images in a digital imaging and communications in medicine (DICOM)
329 format and use an open-platform image analysis software.
330

331 **5.   MRI segmentation and data analysis (see Figure 4)**
332

333 5.1.   Drag and drop the Dicom files into the database of an open-platform software to load all
334 the images.
335

336 5.2.   Use the LGE images to visualize contrast uptake in the vessel wall and calculate the area
337 of enhancement as a surrogate marker of endothelial cell leakage.
338

339 5.3.   Select both the MRA and inversion recovery scans. Press **Enter** to load these images side-
340 by-side. Click on the small icon next to the scan name and drag and drop the MRA images onto
341 the LGE images.
342

343 5.4.   Select the option **Re-sample** to re-slice the MRA images using the LGE images as a
344 reference to account for differences in slice thickness.
345

346 5.5.   Click on the small icon next to the scan name. Drag and drop the LGE images onto the
347 MRA images (as in step 5.4 above). From the menu, choose **Image Fusion** to overlay the LGE and
348 MRA images.
349

350 5.6.   From the toolbar, click on **2D Viewer**, and then choose **3D Position Panel**. Use the buttons

351 to manually correct for in-plane shifts to account for potential small displacements because of
352 animal respiration.
353
354 5.7.   Use the **Closed Polygon** tool located in the toolbar to manually segment the visually
355 enhanced segment of the vessel wall. Use the co-registered MRA and LGE images to guide the
356 segmentation.
357
358 5.8.   Segment all the LGE images that encompass the brachiocephalic artery.
359
360 NOTE: If the enhancement of the vessel wall has a diffused or patchy appearance, segment those
361 individually in each slice.
362
363 5.9.   Click on the **Plugins** button in the toolbar and choose **ROI Tools**, and then **Export ROIs** to
364 export the segmented area (mm^2) for each region of interest (ROI) in a spreadsheet.
365
366 5.10.   Sum the area of each slice to calculate the total area of enhancement in the
367 brachiocephalic artery in the spreadsheet.
368
369 NOTE: The total area of enhancement can be used as a quantitative marker of endothelial
370 permeability.
371
372 5.11.   Use the T1 maps that are automatically generated on the MRI scanner computer to
373 calculate the mean T1 value of the vessel wall that reflects the amount of uptake of gadofosveset
374 into the vessel wall—this is another quantitative marker of endothelial permeability.
375
376 5.12.   Load the MRA and T1 map images and follow a similar approach as described above (steps
377 5.3–5.9) to segment the vessel wall and extract the T1 values (ms).
378
379 5.13.   In a spreadsheet, invert the T1 values and multiply by 1000 to calculate the relaxation
380 time R1 = $^1/_{T1}$ in seconds. Calculate the mean R1 for all slices covering the brachiocephalic artery
381 in each animal.
382
383 5.14.   Load the phase contrast angiography images and velocity maps to calculate the changes
384 in the area of the vessel and blood flow velocity, respectively, during the cardiac cycle.
385
386 5.15.   Segment both the images acquired before and after injection of acetylcholine to calculate
387 endothelial-dependent vasoreactivity, a surrogate marker of endothelial (dys)function.
388
389 5.16.   Use the semi-automated **Grow Region** tool available in the ROI tab or use the **Closed**
390 **Polygon** option available in the toolbar (as described in step 5.7) to segment the lumen area
391 (mm^2) of the brachiocephalic artery in the angiography images.
392
393 NOTE: The semi-automated tool uses pixel thresholding to cluster pixels encompassing the blood

394   pool based on their signal intensity.

395

396   5.17.   Use the **Close Polygon** tool to segment the corresponding blood flow velocity encoded

397   maps to calculate the blood flow velocity (cm/s).

398

399   5.18.   Export the lumen area (mm^2) and blood flow velocity (cm/s) in a spreadsheet (as

400   described in step 5.9) and identify those that correspond to the end-diastolic (maximum area)

401   and end-systolic (minimum area) cardiac phases.

402

403   5.19.   Use the tabulated spreadsheet to calculate the endothelium-dependent vasodilation

404   (calculate the percentage change in the end-diastolic (ED) lumen area and blood flow velocity

405   pre- and post-injection of acetylcholine). Use the following formulas:

406

407    $\%\Delta_{\text{area change}} = \dfrac{(\text{EDarea post} - \text{EDarea pre})}{\text{ED area pre}} * 100$

408

409    $\%\Delta_{\text{flow change}} = \dfrac{(\text{EDflow post} - \text{EDflow pre})}{\text{EDflow pre}} * 100$

410

411   5.20.   For each animal, tabulate the corresponding data derived from the LGE images, T1 maps,

412   and the acetylcholine test in statistical software for analysis.

413

414   **REPRESENTATIVE RESULTS:**

415   In this report, the application of a **Q**uantitative **M**RI method is demonstarted to measure

416   **E**ndo**T**helial pe**R**meab**I**lity and (dys)fun**C**tion (qMETRIC) in the brachiocephalic artery of

417   atherosclerotic ApoE$^{-/-}$ mice. This method provides direct and quantifiable data of two markers

418   of endothelial damage — permeability and (dys)function, which can be extracted from *in vivo*

419   vessel wall scans acquired within a single imaging session. First, LGE are used to measure the area

420   of vessel wall enhancement (mm^3), and T1 (or R1) maps are used to quantify the relaxation rate

421   of the vessel wall (s^{-1}) after administration of gadofosveset, both surrogate markers of

422   permeability (see **Figure 5** for representative results). The vessel wall R1 relaxation rate ranged

423   from 2.42 s^{-1} ± 0.35 s^{-1} to 3.45 s^{-1} ± 0.54 s^{-1} to 3.83 s^{-1} ± 0.52 s^{-1} at 4 weeks, 8 weeks, and 12 weeks

424   of a high-fat diet, respectively. Conversely, wild-type (R1 = 2.15 ± 0.34 s^{-1}) and statin-treated

425   ApoE$^{-/-}$ (R1 = 3.0 ± 0.65 s^{-1}) mice showed less enhancement. In ApoE$^{-/-}$ mice fed with a high-fat

426   diet for up to 12 months, the study shows with histological analysis, Evans Blue dye, and electron

427   microscopy that endothelial permeability increases during atherosclerosis progression, which

428   was in agreement with increased LGE vessel wall volume, increased change in vessel wall R1

429   relaxivity, and paradoxical vasoconstriction after acetylcholine injection[5]. Conversely, statin and

430   other endothelium-targeting treatments decreased endothelial permeability and plaque size,

431   which was reflected in smaller LGE volume, lower R1 values[5,7], and improved vasodilation.

432   Mechanistically, gadofosveset binds reversibly to serum albumin. This results in a 5–6-fold

433   increase in the T1 relaxivity of the probe[29]—making it detectable by MRI with high sensitivity.

434   Here, the study shows that bound to albumin, the uptake of the probe reflects endothelial

435   leakiness because it correlates with the uptake of Evan's blue dye—a gold-standard *ex vivo*

436   method of quantifying endothelial leakage (**Figure 5**) — and wider tight gap junctions[5]. Secondly,

437 a simple test is demonstrated to measure endothelial (dys)function, in response to acetylcholine.
438 In control vessels, acetylcholine causes endothelium-depended vascular relaxation leading to
439 increased arterial area/volume and blood flow. To measure endothelial (dys)function, ECG-
440 triggered angiography images acquired before and after administration of acetylcholine were
441 used. The study calculates the change in the end-diastolic (or volume) of the vessel lumen before
442 and after the administration of acetylcholine. It was found that, unlike normal vessels that
443 vasodilate in response to acetylcholine, atherosclerotic vessels demonstrate decreased
444 endothelial-dependent vasodilatory function that manifests either as a reduced change in vessel
445 area (or volume) or even paradoxical vasoconstriction of the vessel (**Figure 5**). Interestingly, statin
446 treatment improved vasodilatory properties of the endothelium[13].
447
448 **FIGURE AND TABLE LEGENDS:**
449 **Figure 1: Workflow to image endothelial permeability and (dys)function in atherosclerotic**
450 **mice.** (**A–B**) Mice are first anesthetized and then injected with the albumin contrast agent. (**C**)
451 Mice are then transferred onto an MRI coil, where ECG pads are used to monitor cardiac activity.
452 (**D–E**) MRI images are acquired to quantify endothelial permeability and (dys)function that are
453 subsequently analyzed using an open-platform software (created with BioRender.com).
454
455 **Figure 2: Animal positioning and ECG monitoring to image endothelial permeability and**
456 **(dys)function using a clinical 3 Tesla MRI scanner.** (**A–B**) The animal is positioned prone on a
457 surface coil and maintained anesthetized using inhalable isoflurane. Sandbags are used to
458 stabilize the imaging platform. (**C–D**) ECG pads are placed on the paws and connected to a clinical
459 ECG module to record cardiac activity.
460
461 **Figure 3: MRI planning and acquisition of images to quantify endothelial permeability and**
462 **(dys)function in the brachiocephalic artery of atherosclerotic mice.** (**A**) Scout images are
463 acquired to identify the anatomical region between the aortic root and the carotid arteries. (**B**)
464 The MR angiogram is used to visualize the vasculature and plan the subsequent scans. (**C**) Look-
465 Locker images are acquired at the level of the brachiocephalic artery to determine the suitable
466 time delay to null the signal from the blood in the subsequent later gadolinium enhancement
467 images (LGE). (**D**) LGE images provide a visual assessment of vessel wall enhancement. (**E**) T1
468 mapping is used to calculate the vessel wall relaxation rate that is indicative of the concentration
469 of gadolinium. (**F**) The endothelium-depended vasodilating properties of the vessel wall are
470 quantified after the administration of acetylcholine.
471
472 **Figure 4: Image segmentation and analysis to quantify endothelial permeability and**
473 **(dys)function in the brachiocephalic artery of atherosclerotic mice.** (**A**) The vessel wall is
474 manually segmented on the LGE images to quantify the area/volume of contrast uptake. (**B**) The
475 vessel wall is segmented on the T1 mapping to calculate the vessel wall relaxation rate. (**C**) The
476 vessel wall segmented on the MR angiograms and blood flow encoded images is used to study
477 the vasodilating properties of the vessel wall by calculating the changes in volume and blood flow
478 after administration of acetylcholine.
479
480 **Figure 5: Quantitative imaging of endothelial permeability and (dys)function (qMETRIC) in**

atherosclerotic mice. (**A**) LGE images and R1 relaxation maps show increased uptake of the albumin-binding contrast agent within the vessel wall during atherosclerosis progression and the improvement after statin treatment. Imaging data are corroborated by the accumulation of Evan's blue dye, an albumin-binding dye, *ex vivo*. (**B**) Changes in the vasodilating properties of the vessel wall, in response to acetylcholine administration, allow quantification of endothelial-dependent vasodilation. Control vessels vasodilate, whereas atherosclerotic vessels vasoconstrict in response to acetylcholine, suggestive of endothelial damage. Treatment with statin improves endothelial damage. The terms "wks" and "HFD" in the figure represents "weeks" and "high-fat diet", respectively. This figure has been modified from Phinikaridou, A. et al.[5].

DISCUSSION:

Determining vascular endothelial health is an attractive imaging biomarker that can potentially be used to diagnose atherosclerotic-related risk and to monitor treatment effects. The qMETRIC protocol outlined here can be used to reproducibly quantitate endothelial permeability/leakiness and (dys)function in a comprehensive, fast, and clinically applicable MRI protocol. Such an approach can provide a simpler alternative or complementary tool to existing DCE-MRI protocols for quantifying endothelial permeability. It can also provide a non-invasive tool for direct assessment of endothelial (dys)function in vascular beds, such as the coronary and carotid arteries, instead of using either invasive techniques or surrogate measurements in peripheral arteries that are less severely affected by the disease. Measuring endothelial permeability using this method allows coverage of the aorta, the aortic arch, and the brachiocephalic and carotid arteries at high spatial resolution (0.1 mm for the LGE images and 0.22 mm for T1 mapping) that is crucial for accurate segmentation of the vessel wall in rodents. Analysis of the images can be carried out using an open-source platform and requires only a simple segmentation of the vessel wall without the need for complex pharmacokinetic modeling. Importantly, this protocol can be adapted to be used in a number of different commercially available scanners and can be extended to be used in different animal models and also humans. Although this protocol describes the methodology using a clinical scanner setup, the MRI protocols can also be implemented when using high-field small animal scanners. These scanners frequently offer inversion recovery, T1 mapping, and angiography protocols that can be used or can be programmed in collaboration with the scanner manufacturers.

To obtain accurate and reproducible results, particular attention should be paid to some critical steps of the protocol. Firstly, when imaging small animals in a clinical scanner, suitable and custom-made receiver coils are necessary to maximize the signal-to-noise ratio for high image quality. The animal positioning on the coil is also crucial, avoiding separation and air-filled spaces between the animal and the coil to improve the signal-to-noise ratio. For this reason, the anatomical area of interest should be placed in the center of the coil, and then moved to the isocenter of the magnet to expose them to the magnetic field with maximum homogeneity. Secondly, a stable, strong, and accurate ECG signal is paramount for reliable imaging triggering/gating. This is important for consistent excitation of the magnetization and the timing of the image acquisition window at specific time points and for acquiring accurate time-resolved images that include the end-diastolic phase for the functional test. Small animal pad-based or needle-based electrodes are more suitable options when used at higher-field strength scanners,

which are better shielded compared to clinical scanners. When these options are used at clinical field scanners, the ECG cables need to be warped together to avoid the formation of resonant circuits at the MRI Lamour frequency that may deteriorate the ECG signal during the pulse sequence. Alternatively, we propose the use of the ECG module and pads used for human scans with adjustment of the pad size to that of the mouse paw and extra stabilization of the pads with tape to improve conductivity. Thirdly, when acquiring LGE images while the contrast agent is still circulating in the bloodstream, it is crucial to choose the correct nulling time to efficiently suppress the blood pool to delineate the vessel wall. A Look-locker sequence must be run before every LGE sequence, and the inversion delay time needs to be adjusted accordingly. Fourthly, for accurate and precise T1 mapping using a modified look-locker inversion recovery (MOLLI) sequence, the proposed image acquisition scheme should be implemented to cover a range of inversion delays ranging at least from 20 ms to 2000 ms to capture the short and long T1 species. Lastly, segmentation of MRI data must be rigorous and strict criteria applied to avoid intra and/or inter-observer biases in the area/volume and T1 value calculations.

Unlike DCE-MRI, the procedure described here does not provide kinetic data of the wash-in and wash-out of the contrast agent in the vessel wall. Rather, it provides a snapshot of endothelial permeability at a specific time point after injection of the albumin-binding contrast agent, gadofosveset. However, the extracted quantitative data from these time-points highly correlated with other albumin-dyes, such as Evan's blue dye, which is considered a gold-standard to measure endothelial permeability and increased endothelial gap-junction width. Mechanistically, both the albumin-bound and unbound-fraction of gadofosveset are small enough to pass through breaks in the endothelial junctions and lead to MRI signal enhancement. Additionally, it is possible that the unbound-fraction may also bind to intraplaque albumin after it enters the vessel wall and results in signal enhancement. It was observed that the relaxivity of the vessel wall is r_1 ≈17 mmol/L/s, when gadofosveset is injected at a clinical dose. This value is closer to that reported for the albumin-bound fraction (r_1 ≈25 mmol/L/s) compared to the free-fraction (r_1 ≈6.6 mmol/L/s)[5,29].

Future applications of this imaging method include basic science studies in different animal models and other arterial segments and the use of this method to assess for biological responses to existing or novel pharmaceutical agents. Studies can be performed either cross-sectionally or longitudinally to gather mechanistic and outcome data, respectively. The straightforward workflow makes this approach accessible and clinically applicable for use in humans also. Adaptation of this method for imaging human carotid and peripheral arteries is more imminent, but the application of this method for imaging the coronary arteries requires further advancements in image acquisition, reconstruction, and motion-correction that are currently being developed[30,31].
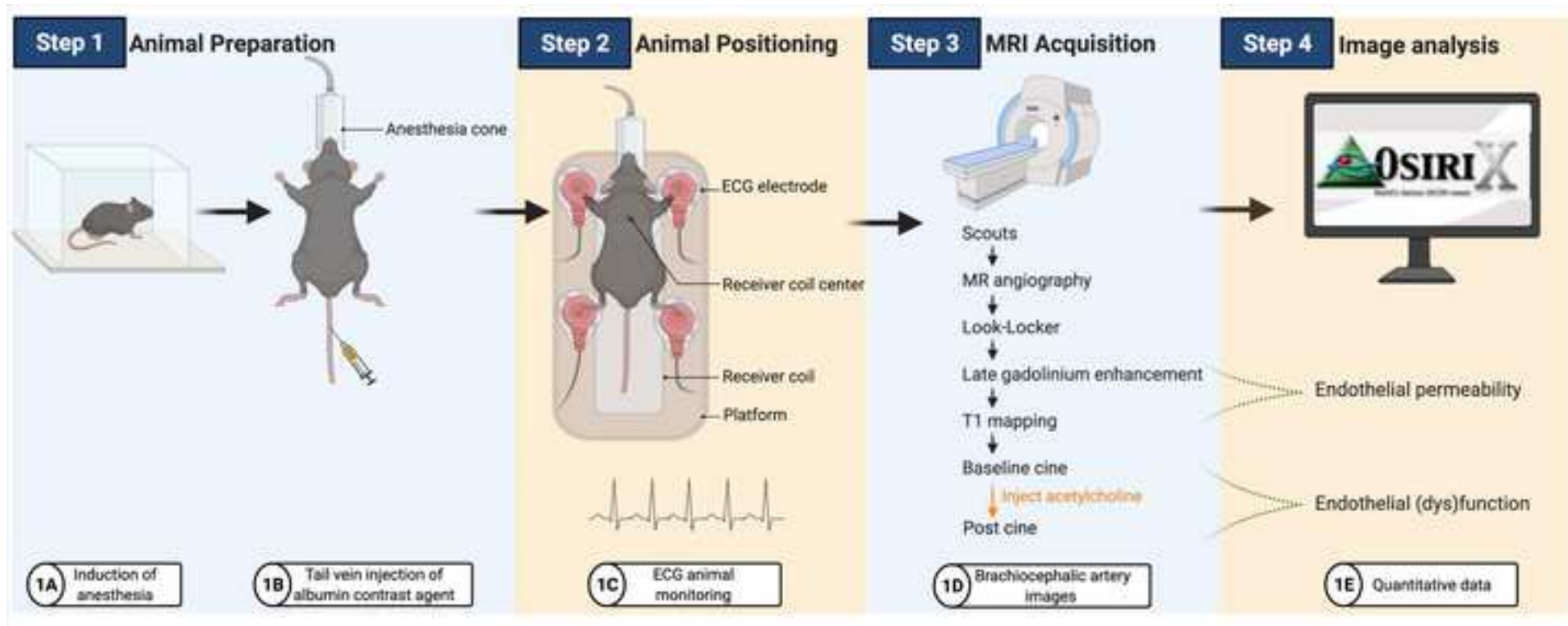
575
576 **DISCLOSURES:**
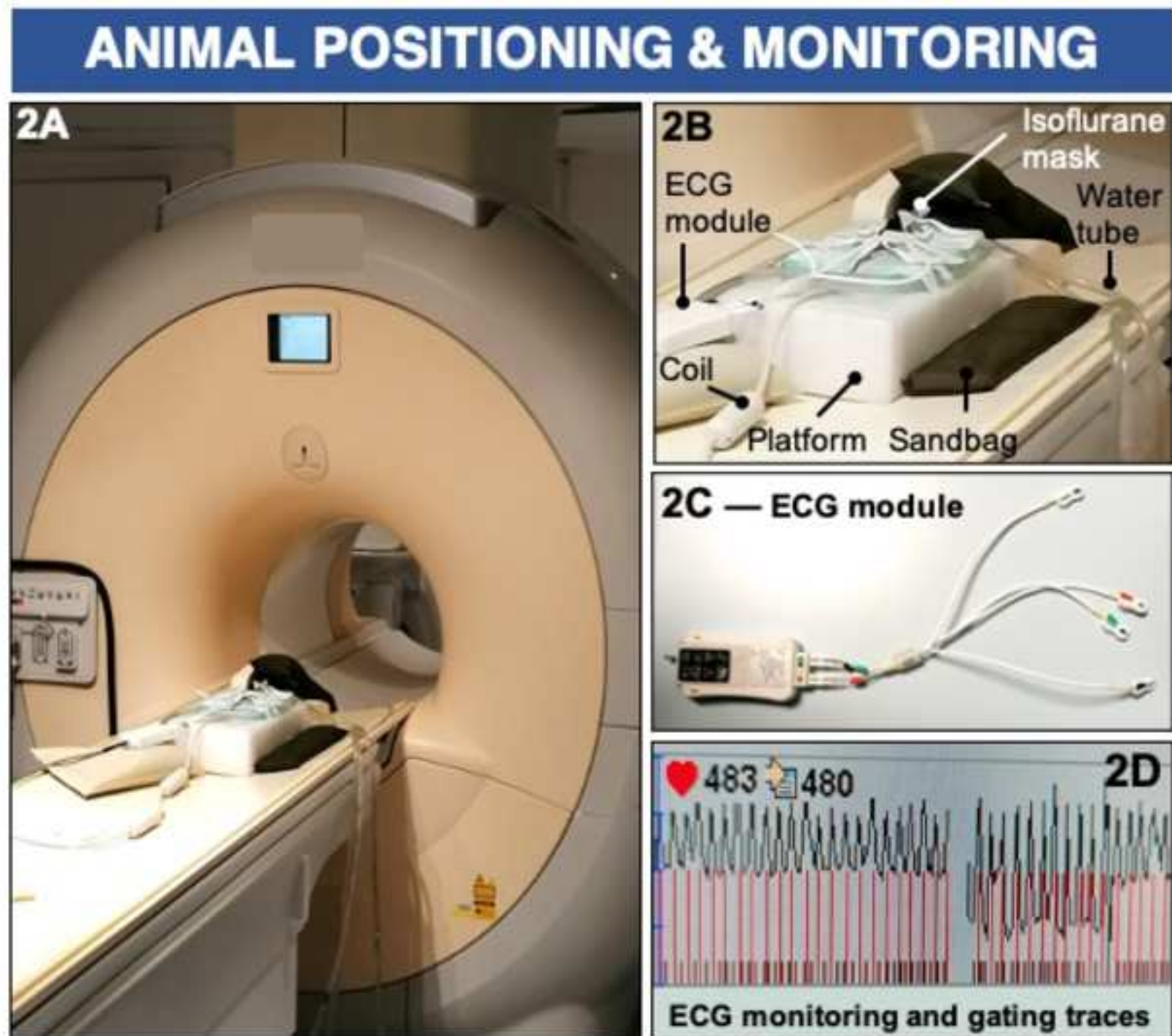577 The authors have nothing to disclose.
578

579 **REFERENCES**:
580 1.   Lloyd-Jones, D. M. et al. Defining and setting national goals for cardiovascular health
581 promotion and disease reduction: The American heart association's strategic impact goal through
582 2020 and beyond. *Circulation*. **121** (4), 586–613 (2010).
583 2.   Davignon, J., Ganz, P. Role of endothelial dysfunction in atherosclerosis. *Circulation*. **109**
584 (23 Suppl 1), III27–32 (2004).
585 3.   Ludmer, P. L. et al. Paradoxical vasoconstriction induced by acetylcholine in
586 atherosclerotic coronary arteries. *New England Journal of Medicine*. **315** (17), 1046–1051 (1986).
587 4.   Crauwels, H. M., Van Hove, C. E., Holvoet, P., Herman, A. G., Bult, H. Plaque-associated
588 endothelial dysfunction in apolipoprotein E-deficient mice on a regular diet. Effect of human
589 apolipoprotein AI. *Cardiovascular Research*. **59** (1), 189–199 (2003).
590 5.   Phinikaridou, A. et al. Non-invasive magnetic resonance imaging evaluation of endothelial
591 permeability in murine atherosclerosis using an albumin-binding contrast agent. *Circulation*. **126**
592 (6), 707–719 (2012).
593 6.   Phinikaridou, A. et al. Increased vascular permeability measured with an albumin-binding
594 magnetic resonance contrast agent is a surrogate marker of rupture-prone atherosclerotic
595 plaque. *Circulation; Cardiovascular Imaging*. **9** (12) (2016).
596 7.   Phinikaridou, A., Andia, M. E., Passacquale, G., Ferro, A., Botnar, R. M. Noninvasive MRI
597 monitoring of the effect of interventions on endothelial permeability in murine atherosclerosis
598 using an albumin-binding contrast agent. *Journal of the American Heart Association*. **2** (5),
599 e000402 (2013).
600 8.   Sluimer, J. C. et al. Thin-walled microvessels in human coronary atherosclerotic plaques
601 show incomplete endothelial junctions relevance of compromised structural integrity for
602 intraplaque microvascular leakage. *Journal of the American College of Cardiology*. **53** (17), 1517–
603 1527 (2009).
604 9.   Rubenfire, M., Cao, N., Smith, D. E., Mosca, L. Carotid artery reactivity to isometric hand
605 grip exercise identifies persons at risk and with coronary disease. *Atherosclerosis*. **160** (1), 241–
606 248 (2002).
607 10.   Nguyen, P. K., Meyer, C., Engvall, J., Yang, P., McConnell, M. V. Non-invasive assessment
608 of coronary vasodilation using cardiovascular magnetic resonance in patients at high risk for
609 coronary artery disease. *Journal of Cardiovascular Magnetic Resonance*. **10**, 28 (2008).
610 11.   Terashima, M. et al. Impaired coronary vasodilation by magnetic resonance angiography
611 is associated with advanced coronary artery calcification. *Journal of the American College of*
612 *Cardiology; Cardiovascular Imaging*. **1** (2), 167–173 (2008).

613   12.   Hays, A. G. et al. Non-invasive visualization of coronary artery endothelial function in
614   healthy subjects and in patients with coronary artery disease. *Journal of the American College of*
615   *Cardiology*. **56** (20), 1657–1665 (2010).
616   13.   Hirooka, Y. et al. Effect of L-arginine on acetylcholine-induced endothelium-dependent
617   vasodilation differs between the coronary and forearm vasculatures in humans. *Journal of the*
618   *American College of Cardiology*. **24** (4), 948–955 (1994).
619   14.   Takase, B. et al. Endothelium-dependent flow-mediated vasodilation in coronary and
620   brachial arteries in suspected coronary artery disease. *American Journal of Cardiology*. **82** (12),
621   1535–1539 (1998).
622   15.   Al-Badri, A., Kim, J. H., Liu, C., Mehta, P. K., Quyyumi, A. A. Peripheral microvascular
623   function reflects coronary vascular function. *Arteriosclerosis Thrombosis and Vascular* Biology.
624   39 (7), 1492–1500 (2019).
625   16.   Calcagno, C. et al. Detection of neovessels in atherosclerotic plaques of rabbits using
626   dynamic contrast enhanced MRI and 18F-FDG PET. *Arteriosclerosis Thrombosis and Vascular*
627   *Biology*. **28** (7), 1311–1317 (2008).
628   17.   Lobbes, M. B. et al. Atherosclerosis: contrast-enhanced MR imaging of vessel wall in rabbit
629   model--comparison of gadofosveset and gadopentetate dimeglumine. *Radiology*. **250** (3), 682–
630   691 (2009).
631   18.   Kerwin, W. S., Oikawa, M., Yuan, C., Jarvik, G. P., Hatsukami, T. S. MR imaging of
632   adventitial vasa vasorum in carotid atherosclerosis. *Magnetic Resonance Medicine*. **59** (3), 507–
633   514 (2008).
634   19.   van Hoof, R. H. et al. Vessel wall and adventitial DCE-MRI parameters demonstrate similar
635   correlations with carotid plaque microvasculature on histology. *Journal of Magnetic Resonance*
636   *Imaging*. **46** (4), 1053–1059 (2017).
637   20.   Calcagno, C., Mani, V., Ramachandran, S., Fayad, Z. A. Dynamic contrast enhanced (DCE)
638   magnetic resonance imaging (MRI) of atherosclerotic plaque angiogenesis. *Angiogenesis*. **13** (2),
639   87–99 (2010).
640   21.   van Wijk, D. F. et al. Increasing spatial resolution of 3T MRI scanning improves
641   reproducibility of carotid arterial wall dimension measurements. *Magnetic Resonance Materials*
642   *in Physics, Biology, and Medicine*. **27** (3), 219–226 (2014).
643   22.   Li, B. et al. Turbo fast three-dimensional carotid artery black-blood MRI by combining
644   three-dimensional MERGE sequence with compressed sensing. *Magnetic Resonance Medicine*.
645   **70** (5), 1347–1352 (2013).
646   23.   Fan, Z. et al. Carotid arterial wall MRI at 3T using 3D variable-flip-angle turbo spin-echo
647   (TSE) with flow-sensitive dephasing (FSD). *Journal of Magnetic Resonance Imaging*. **31** (3), 645–
648   654 (2010).
649   24.   Li, X., Huang, W. & Rooney, W. D. Signal-to-noise ratio, contrast-to-noise ratio and
650   pharmacokinetic modeling considerations in dynamic contrast-enhanced magnetic resonance
651   imaging. *Magnetic Resonance Imaging*. **30** (9), 1313–1322 (2012).
652   25.   Heisen, M. et al. The influence of temporal resolution in determining pharmacokinetic
653   parameters from DCE-MRI data. *Magnetic Resonance Medicine*. **63** (3), 811–816 (2010).
654   26.   Chen, H. et al. Scan-rescan reproducibility of quantitative assessment of inflammatory
655   carotid atherosclerotic plaque using dynamic contrast-enhanced 3T CMR in a multi-center study.
656   *Journal of Cardiovascular Magnetic Resonance*. **16**, 51 (2014).
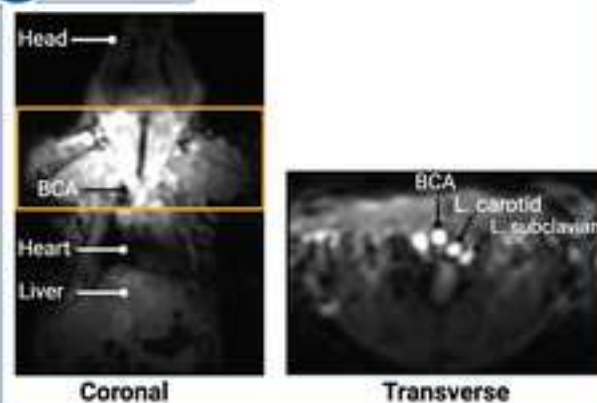
657 27.   Calcagno, C., Vucic, E., Mani, V., Goldschlager, G., Fayad, Z. A. Reproducibility of black
658 blood dynamic contrast-enhanced magnetic resonance imaging in aortic plaques of
659 atherosclerotic rabbits. *Journal of Magnetic Resonance Imaging*. **32** (1), 191–198 (2010).
660 28.   Engel, L. C. et al. Non-invasive imaging of endothelial damage in patients with different
661 HbA1c levels: A proof-of-concept study. *Diabetes*. **68** (2), 387–394 (2019).
662 29.   Caravan, P. et al. The interaction of MS-325 with human serum albumin and its effect on
663 proton relaxation rates. *Journal of the American Chemical Society*. **124** (12), 3152–3162 (2002).
664 30.   Munoz, C. et al. Motion-corrected 3D whole-heart water-fat high-resolution late
665 gadolinium enhancement cardiovascular magnetic resonance imaging. *Journal of Cardiovascular*
666 *Magnetic Resonance*. **22** (1), 53 (2020).
667 31.   Milotta, G. et al. 3D whole-heart isotropic-resolution motion-compensated joint T1 /T2
668 mapping and water/fat imaging. *Magnetic Resonance Medicine*. **84** (6), 3009–3026 (2020).
669
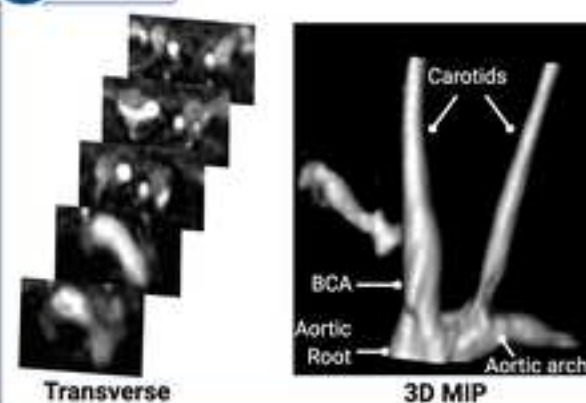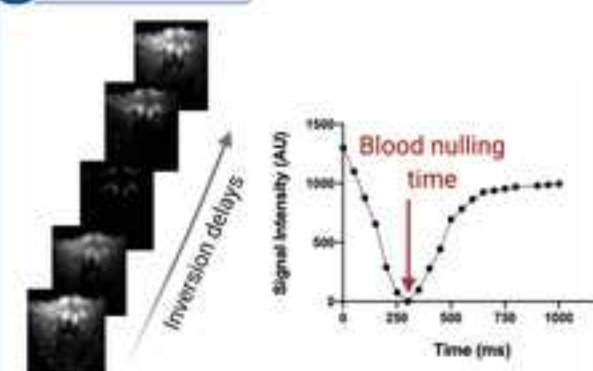
Figure 2　　　　　　　　　　　　　　　　　Click here to access/download;Figure;Fig 2 -revised-2.jpg ⬇

ANIMAL POSITIONING & MONITORING

2A

2B — ECG module, Isoflurane mask, Water tube, Coil, Platform, Sandbag

2C — ECG module

2D — ♥ 483 🫁 480 — ECG monitoring and gating traces

Figure 3

Image Segmentation and Analysis

4A LGE

BCA

Fused LGE & MRA   Segmented LGE

4B T1 mapping

Segmented T1 map

T1 recovery curve

4C Vasodilation test

Pre Ace   Post Ace

segmented EDV (mm³)

Segmented blood flow (cm/s)

Figure 5
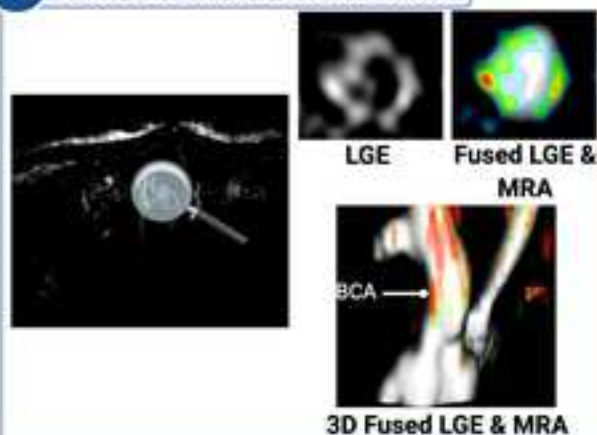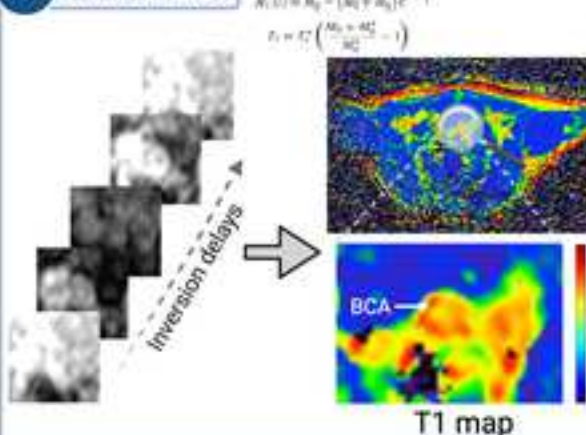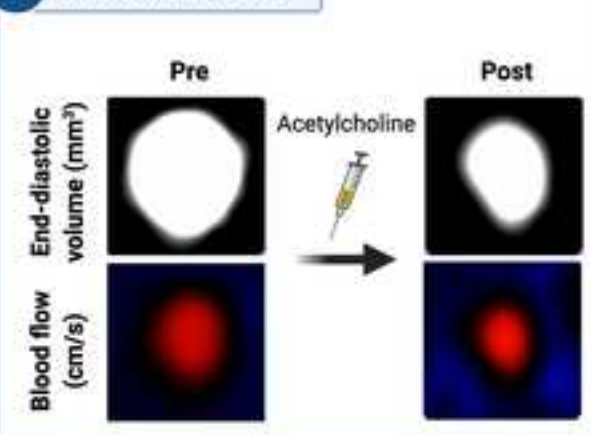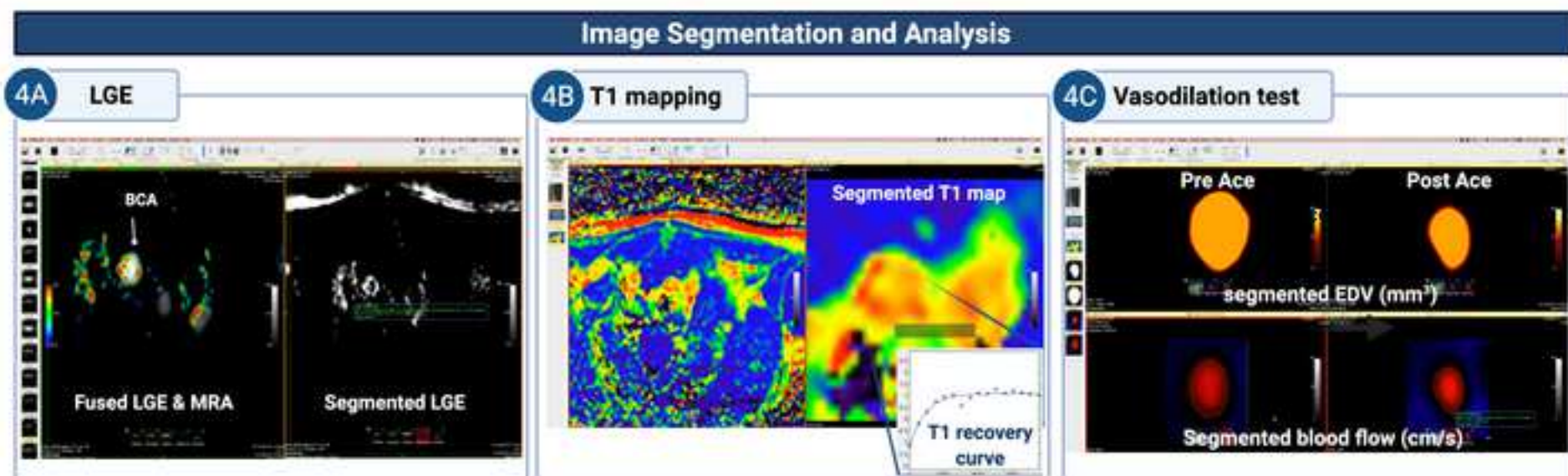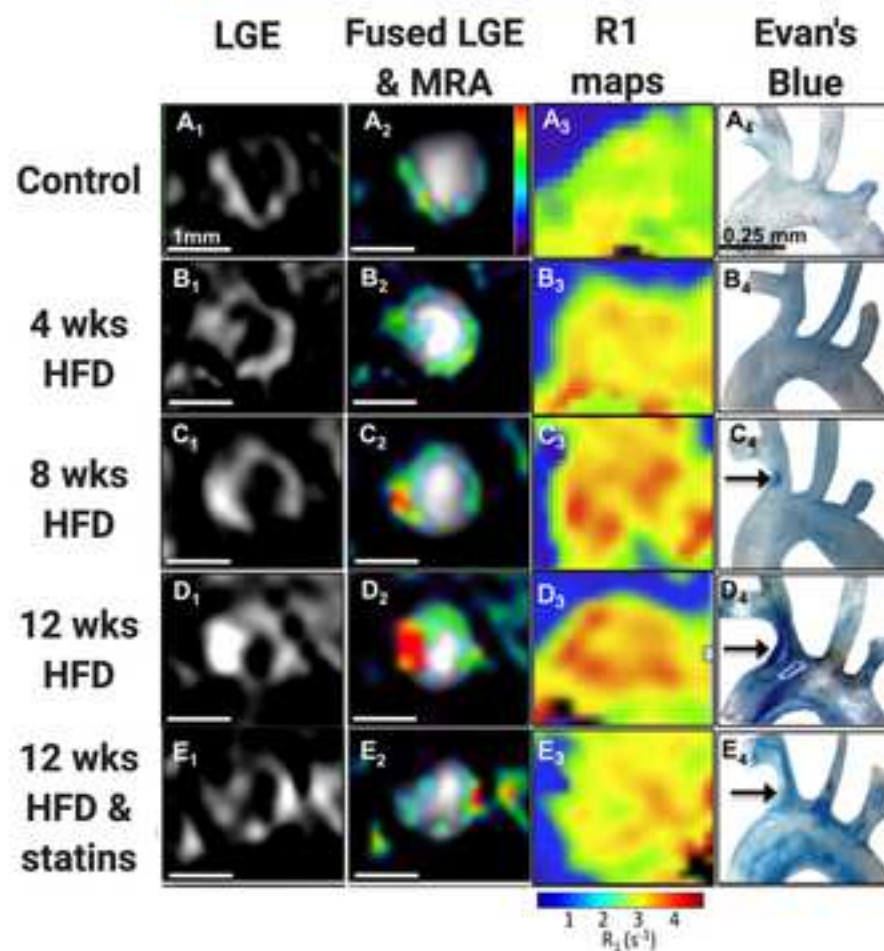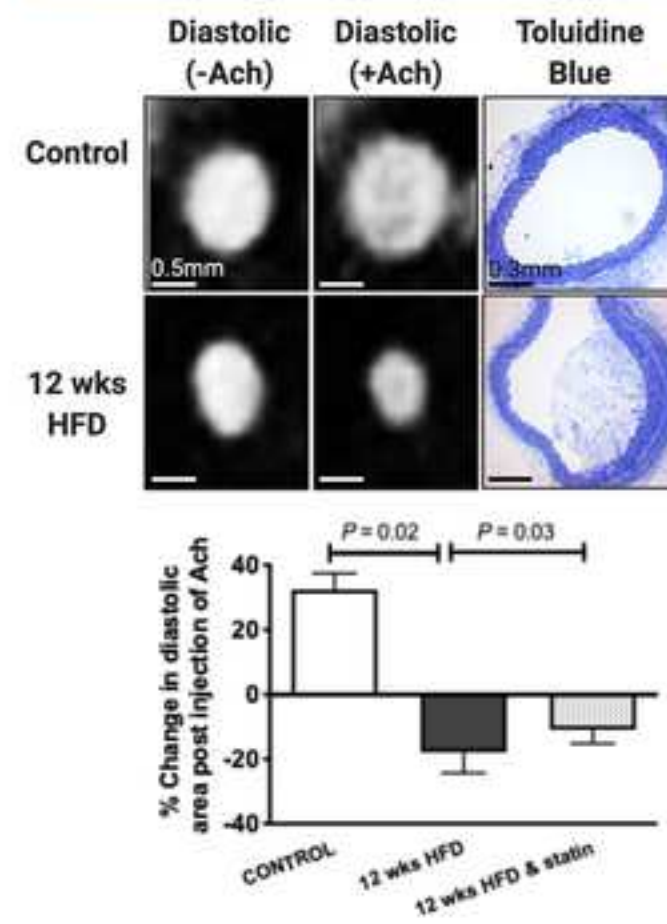
Table 1

TABLE 1: MRI acquisition parameters **Scan / Sequence**
Scout / pilot scan
MRA scan
Look-Locker scan
LGE scan
T1 mapping scan
Phase contrast angiography scan

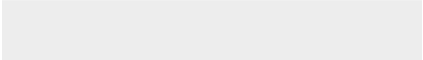| Acquisition parameters |
|---|
| 3D, fast gradient echo
Transverse: FOV = 50 mm x 27 mm x 14 mm, matrix = 96 x 52, in-plane resolution = 0.5 mm x 0.5 mm, slice thickness = 0.5 mm, TR/TE = 15/6.1 ms, flip angle = 30°, averages = 1
Coronal: FOV = 200 mm x 102 mm x 14 mm, matrix = 336 x 173, in-plane resolution= 0.5 mm x 0.5 mm, slice thickness = 0.5 mm, TR/TE = 12/6 ms, flip angle = 30°, averages = 1 |
| 3D fast gradient echo, FOV = 30 mm x 30 mm x 8 mm, matrix = 200 x 200, in-plane resolution =0.15 mm x 0.15 mm, slice thickness = 0.5 mm, TR/TE = 15/6.1 ms, flip angle = 40°, averages = 1 |
| 2D fast gradient echo, FOV = 30 mm x 30 mm, matrix = 80 x 80, in-plane resolution = 0.38 mm x 0.38 mm, slice thickness = 2 mm, TR/TE = 19/8.6 ms, TR between subsequent IR pulses = 1000 ms, and flip angle = 10°, averages = 1. |
| 3D fast gradient echo, FOV = 30 mm x 30 mm x 8 mm, matrix = 304 x 304, in-plane resolution = 0.1mm x 0.1 mm, measured slice thickness = 0.5 mm, slices = 32, TR/TE = 28/8 ms, TR between subsequent IR pulses = 1000 ms, and flip angle = 30°, averages = 1. |
| 3D fast gradient echo , FOV = 36 mm x 22 mm x 8 mm, matrix = 192 x 102, in-plane resolution = 0.18 mm x 0.22 mm, measured slice thickness = 0.5 mm, slices = 16, TR/TE = 9.6/4.9 ms, flip angle = 10°, averages = 1. |
| 2D, fast gradient echo, FOV = 40 mm x 23 mm, matrix = 132 x 77, in-plane resolution = 0.3 mm x 0.3 mm x 1 mm, TR/TE = 9.8/4.9 ms, flip angle = 30°, cardiac phases = 14, averages = 6, flow velocity (foot-head direction) = 30 cm/s. |

Click here to access/download
Table of Materials
Table of Materials-62724_R1.xls

Guy's, King's and St. Thomas'
Faculty of Life Sciences and Medicine
School of Biomedical Engineering and
Imaging Sciences

King's College LONDON

University of London

Dr. Alkystis Phinikaridou, PhD
Senior Lecturer in Imaging Biology
School of Biomedical Engineering
and Imaging Sciences
3rd Floor, Lambeth Wing
St Thomas' Hospital, London SE1 7EH
Tel 020 718 88386, Fax 020 718 85442
Email alkystis.1.phinikaridou@kcl.ac.uk

24-05-2021

RE: "Quantitative MRI of Endothelial Permeability and (Dys)function in Atherosclerosis (JoVE62724)"

Dear Editors and Reviewers,

We would like to thank you for the interest in our work and your insightful comments. We have taken your suggestions under careful consideration and addressed them in our revised manuscript. Below, you will find our responses to the comments that have been raised. We believe that the comments have greatly improved the clarity and aims of the work presented in this manuscript. Our changes are indicated in red in the manuscript. We believe that our work would be of interest to the readers of your journal and we hope it will be considered for publication in JoVE.

Thank you for your kind consideration.

Sincerely yours,

Alkystis Phinikaridou, PhD

Editorial comments:
Changes to be made by the Author(s):

1. Please take this opportunity to thoroughly proofread the manuscript to ensure that there are no spelling or grammar issues.
Answer: We have performed a thorough spell check.

2. Please define all abbreviations during the first-time use.
Answer: We have defined all abbreviations at the point of first used.

3. Please format the manuscript as: paragraph Indentation: 0 for both left and right and special: none, Line spacings: single. Please include a single line space between each step, substep and note in the protocol section. Please use Calibri 12 points
Answer: We have complied with all formatting instructions.

4. JoVE cannot publish manuscripts containing commercial language. Please remove all commercial language from your manuscript and use generic terms instead. All commercial products should be sufficiently referenced in the Table of Materials and Reagents. For example: OsiriX,
Answer: We have removed commercial language from the text.

5. Please revise the following lines to avoid overlap with previously published work: 148-154, 157, 188-189, 191, 198-200, 245-248, 272-274, 288-290, 408-414.
Answer: We have revised the sentences indicated above to avoid duplication with published work.

6. Please ensure that the long Abstract is within 150-300-word limit and clearly states the goal of the protocol.
Answer: The abstract is within the word limit and clearly states the Aim of this protocol.

7. Please ensure that all text in the protocol section is written in the imperative tense as if telling someone how to do the technique (e.g., "Do this," "Ensure that," etc.). The actions should be described in the imperative tense in complete sentences wherever possible. Avoid usage of phrases such as "could be," "should be," and "would be" throughout the Protocol. Any text that cannot be written in the imperative tense may be added as a "Note."
Answer: We have complied with this request.

8. Please adjust the numbering of the Protocol to follow the JoVE Instructions for Authors. For example, 1 should be followed by 1.1 and then 1.1.1 and 1.1.2 if necessary.
Answer: We have complied with this request.

9. The Protocol should contain only action items that direct the reader to do something.
Answer: We have complied with this request.

10. Please ensure that individual steps of the protocol should only contain 2-3 actions sentences per step.
Answer: We have complied with this request.

11. Please ensure you answer the "how" question, i.e., how is the step performed?
Answer: We have complied with this request.

12. 1.2: Please include volume and concentration of the solution prepared?
We have change the sentence to read "Load a 29G needle insulin syringe with the right volume of the contrast agent (gadofosveset trisordium) to achieve a dose of (0.03mmol/kg). Keep the injection volume between 50-150µl"

13. Please use the degree symbol (˚) and do not superscript 0 or O.
Answer: We have made the recommended change.

14. Anesthesia steps cannot be filmed.
Answer: We have removed this from the content to be filmed.

15. 4.1: How is this done?
Answer: We have changed the sentence to read "Run the standard calibrations for the MRI system by starting a scout scan"

16. 5: How do you perform each step? Do you perform any button clicks, knob turns, etc? Do you use any command lines? Please include all actions.
Answer: We have changed all relevant sentences in "MRI Segmentation and Data Analysis" section to include specific instructions on how to perform this work in lines 275-338.

17. There is a 10-page limit for the Protocol, but there is a 3-page limit for filmable content.
Answer: Please highlight 3 pages or less of the Protocol (including headings and spacing) that identifies the essential steps of the protocol for the video, i.e., the steps that should be visualized to tell the most cohesive story of the Protocol.
Answer: We have condense the filmable content into 3-pages.

18. Please ensure all figures are referenced in order.
Answer: We have complied with this request.

19. Please ensure the results are described in the context of the presented technique. e.g., how do these results show the technique, suggestions about how to analyse the outcome, etc. Data from both successful and sub-optimal experiments can be included.
Answer: We have complied with this request.

20. Please obtain explicit copyright permission to reuse any figures from a previous publication. Explicit permission can be expressed in the form of a letter from the editor or a link to the editorial policy that allows re-prints. Please upload this information as a .doc or .docx file to your Editorial Manager account. The Figure must be cited appropriately in the Figure Legend, i.e. "This figure has been modified from [citation]."
Answer: We have permission from the publisher to re-use content and we will upload the document on the JoVE website at the time of resubmission.

21. Please include a title and a description of each figure and/or table. All figures and/or

tables showing data must include measurement definitions, scale bars, and error bars (if applicable). Please include all the Figure Legends together at the end of the Representative Results in the manuscript text.
Answer: We have added all the Figure legends at the end of the Representative Results section.

22. Please do not abbreviate the journal titles in the references section.
Answer: We have changed the formatting as requested.

23. Figure 2: Please remove the commercial term shown on the scanner.
Answer: We have removed the commercial term from Figure 2.

24. Table 1: Please upload it as .xlsx file instead.
Answer: We have uploaded the table in an .xlsx format

25. Please sort the materials table in alphabetical order.
Answer: We have changed it as requested.

Reviewers' comments:

Reviewer #1:

Manuscript Summary:

Measurements of endothelial dysfunction are highly relevant in the field of (pre-)clinical atherosclerosis imaging, but robust protocols are indeed lacking. Therefore, this manuscript, presented by an expert lab in this field, is a very valuable contribution to the existing literature on this topic. The protocol is described in sufficient detail in order for others to reproduce the methodology, including sequence parameters and specific timings of individual sequences following contrast agent injection. Also, the use of open-source software facilitates the analysis of the data. I have one major and a few minor comments that the authors should consider to further improve the manuscripts.

Major Concerns:

1. The Introduction and final sentence of the discussion mention possible translational to clinical studies, but this not substantiated by literature and I think this is very optimistic at this stage. This reviewer believes the authors should present their protocol solely in the context of preclinical imaging and that a limit clinical translation to the knowledge that can be obtained from preclinical studies.

Answer: We thank the reviewer for this comment. We have changed the last sentence of the introduction to read "The straightforward workflow makes this approach more accessible to the cardiovascular imaging community" eliminating the statement that this method is more clinically applicable. We have also deleted the last sentence of the Discussion "Ultimately imaging endothelial permeability and function in a single scan may allow diagnosis, guide treatment and monitor outcomes in patients at risk of atherosclerosis using a precision-medicine approach".

2. In the Results section, outcomes for R1 should also be presented quantitatively to give the reader a feeling of the spread in R1 values that can be expected for a group if animals. We have added the following sentence in the results section to give the range of R1 values. "The vessel wall R1 relaxation rate ranged from 2.42 ± 0.35 s^{-1} to 3.45 ± 0.54 s^{-1} to 3.83 ± 0.52s^{-1}

at 4,8, and 12 weeks of high-fat diet, respectively. Conversely, wild-type (R_1=2.15±0.34) and statin-treated ApoE$^{-/-}$ (R_1=3.0±0.65) mice showed less enhancement".

Minor Concerns:
Step 4.1: Consider using 'calibrations' instead of 'adjustments'.
Answer: We have accepted the reviewer's suggestion. The sentence now reads "Run the standard calibrations for the MRI system by starting a scout scan".

Step 4.2: A heart-beat of 300 beats/min at 37 degrees Celcius is quite low for mice. Please consider changing this to 450-600 beats/min.
Answer: We thank the reviewer for this comment. We have changed the range to 400-600 beats per min.

Step 4A8: It is unclear why the heart beat has to be set to 60BMP. I assume this is because the Look-Locker can only be executed in a 'cardiac triggered', although the acquisition is not truly triggered to the mouse heartbeat. This can be clarified in the manuscript.
Answer: We thank the reviewer for this comment and we agree that the way it was written might have been confusing**.** To address this comment we have change the sentence in section 4.1.2 and 4.1.6 to read as "Set the heart rate to 60bpm, when using a simulated ECG signal, or set a blanking period to ensure that the inversion recovery pulse between subsequent inversion recovery pulses is 1000ms when using the recorded ECG signal"

Step 4B3: Considering imaging is performed on a clinical scanner, can retrospective gating cope with the high heart rate of the mouse?
Answer: We thank the reviewer for this comment. To overcome limitations related to increased heart rates in small rodents when using a clinical scanner we use a "patch" that allows for heart rates higher than 250bpm and faster switching gradients.

Step 4.9: What if the system does not generate these maps. Can the authors mention the equations (or refer to literature) needed to generate such maps for other users.
Answer: This is an important point and to address it we have added the following **information in section 4.1.9 "**The equations used to generate the T1 parametric maps are:

$$M_z(t) = A - Be^{\frac{-t}{T_1^*}}$$

$$T_1 = T_1^*\left(\frac{B}{A} - 1\right)$$

Step 5.5: Vessel wall segmentation in Osirix is not ideal because one is limited to using a closed polygon shape as ROI. Ideally, inner and outer vessel wall contours are drawn, from which the vessel wall ROI can be formed. Also, this is still a visual assessment. Please include in the Discussion section how these steps can be made reproducible without significant inter-user variability?
Answer: We agree with the reviewer that manual segmentation of the vessel wall depends on a visual assessment and maybe user dependent. However, segmenting the inner and outer contours does not always apply in cases when LGE images may show diffused/patchy enhancement. For this reason, we stated in the Discussion lines 438-439 that "….rigorous

and strict criteria need to be applied in order to avoid intra and/or inter-observer biases in the area/volume and T1 value calculations."

Step 5.11: Why didn't the authors start by creating R1maps in the first place? In this way mean R1 values can be directly calculated on a slice by slice basis or for the entire volume immediately.
Answer: We agree with the reviewer's point. Generation of R1 maps has however not been implemented on the scanner computer yet. For this reason, we generated the R1 values retrospectively by inverting the T1 values.

Discussion: "Determining vascular … treat atherosclerotic-related risk", rephrase such that it is clear that imaging markers are aimed at monitoring treatment effects.
Answer: We have revised the sentence to read: "Determining vascular endothelial health is an attractive imaging biomarker that can potentially be used to diagnose atherosclerotic-related risk and to monitor treatment effects."

Discussion: Include a section in the Discussion that explains how the methodology would be different when using high-field small animal scanners, which are more commonly used in preclinical imaging than clinical scanner setups.
Answer: To address this comment we have added the following sentence in the Discussion: "Although, we describe this methodology using a clinical scanner set up the MRI protocols can also be implemented when using high-field small animal scanners. Theses scanners frequently offer inversion recovery, T1 mapping and angiography protocols that can be used or can be programmed in collaboration with the scanner manufacturers."

Reviewer #2:
Manuscript Summary:
The manuscript by Dr. Phinikaridou and colleagues is a nice effort to collect and summarize a body of work done by authors over more than a decade in this field. The manuscript concisely and accurately describes important imaging protocols that will be helpful to anyone working in the field of imaging of endothelium. Although supposed to be a condensed summary of prior work with a focus on specific protocols, this reviewer feels that there is a need for some editing that would make the manuscript sufficiently dissimilar from previously published works (see below).

Major Concerns:
None

Minor Concerns:
Lines 76-77 are more similar than expected to that in previously published manuscript doi/10.1161/CIRCIMAGING.116.004910
Answer: We have re-phrase this sentence to read as "However, both the function and permeability of the endothelial cells can deteriorate in the presence of cardiovascular risk factors (e.g. smoking, high cholesterol, diabetes, systemic inflammation, oxidative stress) and by blood flow hemodynamic patterns."

Lines 230-248 need some editing to be sufficiently original as compared to previously published abstract at https://cds.ismrm.org/

Answer: We do not have access to the ismrm link but we have rephrased the sentences to avoid duplications as requested.

Lines 408-419 are more similar than expected to that in previously published manuscript DOI: 10.1161/CIRCULATIONAHA.112.092098

"revised November 2017" is indicated in the footer of the manuscript? Is this a part of previous submission? Please explain.

Answer: We have deleted the footer "revised 2017". This was part of the template we revised from the JoVE and it is not part of a previous submission. We have also rephrased the sentences between lines 408-419, to avoid similarities with our previous publication. The section now reads as: "Mechanistically, both the albumin-bound and unbound-fraction of gadofosveset are small enough to pass through breaks in the endothelial junctions and lead to MRI signal enhancement. Additionally, it is possible that the unbound-fraction may also bind to intraplaque albumin after it enters the vessel wall and result in signal enhancement. We have observed that the relaxivity of the vessel wall is $r_1 \approx 17$ mmol/L/s, when gadofosveset is injected at a clinical dose. This value is closer to that reported for the albumin-bound fraction ($r_1 \approx 25$ mmol/L/s) compared to the free-fraction ($r_1 \approx 6.6$ mmol/L/s)[5,29]".

WOLTERS KLUWER HEALTH, INC. LICENSE TERMS AND CONDITIONS

Apr 29, 2021

This Agreement between Alkystis Phinikaridou ("You") and Wolters Kluwer Health, Inc.("Wolters Kluwer Health, Inc.") consists of your license details and the terms and conditionsprovided by Wolters Kluwer Health, Inc. and Copyright Clearance Center.

License Number	5058110817127
License date	Apr 29, 2021
Licensed ContentPublisher	Wolters Kluwer Health, Inc.
Licensed ContentPublication	Circulation
Licensed Content Title	Noninvasive Magnetic Resonance Imaging Evaluation ofEndothelial Permeability in Murine Atherosclerosis Using anAlbumin-Binding Contrast Agent
Licensed Content Author	Alkystis Phinikaridou, Marcelo E. Andia, Andrea Protti, et al
Licensed Content Date	Jun 29, 2012
Licensed Content Volume	126
Licensed Content Issue	6
Type of Use	Journal/Magazine
Requestor type	University/College
Sponsorship	No Sponsorship
Format	Electronic
Portion	Figures/tables/illustrations
Number offigures/tables/illustrations	2
Author of this WoltersKluwer article	Yes
Will you be translating?	No
Will your content bepublished as OpenAccess?	No
Intend to modify/changethe content	No
Title of new article	Quantitative MRI of Endothelial Permeability and (Dys)functionin Atherosclerosis
Lead author	Begona Lavin
Title of targeted journal	JoVE
Publisher	MyJove Corp.
Expected publication date	Jul 2021
Portions	Figure 2 and part of Figure 6
Requestor Location	Alkystis PhinikaridouDivision of Imaging Sciences, The Rayne Institute 4th Floor, Lambeth Wing, St Thomas' Hospital, Lambeth RdPalace London, se1 7eh United Kingdom Attn: Alkystis Phinikaridou

Publisher Tax ID
Total   0.00 GBP
Terms and Conditions
Wolters Kluwer Health Inc. Terms and Conditions

Duration of License: Permission is granted for a one time use only. Rights herein donot apply to future reproductions, editions, revisions, or other derivative works. Thispermission shall be effective as of the date of execution by the parties for themaximum period of 12 months and should be renewed after the term expires.When content is to be republished in a book or journal the validity of thisagreement should be the life of the book edition or journal issue.

When content is licensed for use on a website, internet, intranet, or any publiclyaccessible site (not including a journal or book), you agree to remove thematerial from such site after 12 months, or request to renew your permissionlicense

Credit Line: A credit line must be prominently placed and include: For book content:the author(s), title of book, edition, copyright holder, year of publication; For journalcontent: the author(s), titles of article, title of journal, volume number, issue number,inclusive pages and website URL to the journal page; If a journal is published by alearned society the credit line must include the details of that society.

Warranties: The requestor warrants that the material shall not be used in any mannerwhich may be considered derogatory to the title, content, authors of the material, or toWolters Kluwer Health, Inc.

Indemnity: You hereby indemnify and hold harmless Wolters Kluwer Health, Inc. andits respective officers, directors, employees and agents, from and against any and allclaims, costs, proceeding or demands arising out of your unauthorized use of theLicensed Material

Geographical Scope: Permission granted is non-exclusive and is valid throughout theworld in the English language and the languages specified in the license.

Copy of Content: Wolters Kluwer Health, Inc. cannot supply the requestor with theoriginal artwork, high-resolution images, electronic files or a clean copy of content.

Validity: Permission is valid if the borrowed material is original to a Wolters KluwerHealth, Inc. imprint (J.B Lippincott, Lippincott-Raven Publishers, Williams &Wilkins, Lea & Febiger, Harwal, Rapid Science, Little Brown & Company, Harper &Row Medical, American Journal of Nursing Co, and Urban & Schwarzenberg - English Language, Raven Press, Paul Hoeber, Springhouse, Ovid), and theAnatomical Chart Company

Third Party Material: This permission does not apply to content that is credited topublications other than Wolters Kluwer Health, Inc. or its Societies. For imagescredited to non-Wolters Kluwer Health, Inc. books or journals, you must obtainpermission from the source referenced in the figure or table legend or credit linebefore making any use of the image(s), table(s) or other content.

Adaptations: Adaptations are protected by copyright. For images that have beenadapted, permission must be sought from the rightsholder of the original material andthe rightsholder of the adapted material

10. **Modifications:** Wolters Kluwer Health, Inc. material is not permitted to be modifiedor adapted without written approval from Wolters Kluwer Health, Inc. with theexception of text size or color. The adaptation should be credited as follows: Adaptedwith permission from Wolters Kluwer Health, Inc.: [the author(s), title of book,edition, copyright holder, year of publication] or [the author(s), titles of article, title ofjournal, volume number, issue number, inclusive pages and website URL to thejournal page].

11. **Full Text Articles:** Republication of full articles in English is prohibited.

12. **Branding and Marketing:** No drug name, trade name, drug logo, or trade logo can beincluded on the same page as material borrowed from *Diseases of the Colon &Rectum, Plastic Reconstructive Surgery, Obstetrics & Gynecology (The GreenJournal), Critical Care Medicine, Pediatric Critical Care Medicine, the AmericanHeart Association publications and the American Academy of Neurology publications.*

13. **Open Access:** Unless you are publishing content under the same Creative Commonslicense, the following statement must be added when reprinting material in OpenAccess journals: "The Creative Commons license does not apply to this content. Useof the material in any format is prohibited without written permission from thepublisher, Wolters Kluwer Health, Inc. Please contact permissions@lww.com forfurther information."

14. **Translations:** The following disclaimer must appear on all translated copies: WoltersKluwer Health, Inc. and its Societies take no responsibility for the accuracy of thetranslation from the published English original and are not liable for any errors whichmay occur.

15. **Published Ahead of Print (PAP):** Articles in the PAP stage of publication can becited using the online publication date and the unique DOI number.i. Disclaimer: Articles appearing in the PAP section have been peer-reviewed andaccepted for publication in the relevant journal and posted online before printpublication. Articles appearing as PAP may contain statements, opinions, andinformation that have errors in facts, figures, or interpretation. Any finalchanges in manuscripts will be made at the time of print publication and will bereflected in the final electronic version of the issue. Accordingly, WoltersKluwer Health, Inc., the editors, authors and their respective employees are notresponsible or liable for the use of any such inaccurate or misleading data,opinion or information contained in the articles in this section.

16. **Termination of Contract:** Wolters Kluwer Health, Inc. must be notified within 90days of the original license date if you opt not to use the requested material.

17. **Waived Permission Fee:** Permission fees that have been waived are not subject tofuture waivers, including similar requests or renewing a license.

18. **Contingent on payment:** You may exercise these rights licensed immediately uponissuance of the license, however until full payment is received either by the publisheror our authorized vendor, this license is not valid. If full payment is not received on atimely basis, then any license preliminarily granted shall be deemed automaticallyrevoked and shall be void as if never granted. Further, in the event that you breach anyof these terms and conditions or any of Wolters Kluwer Health, Inc.'s other billing andpayment terms and conditions, the license is automatically revoked and shall be voidas if never granted. Use of materials as described in a revoked license, as well as anyuse of the materials beyond the scope of an unrevoked license, may constitutecopyright infringement and publisher reserves the right to take any and all action toprotect its copyright in the materials.

19. **STM Signatories Only:** Any permission granted for a particular edition will apply tosubsequent editions and for editions in other languages, provided such editions are forthe work as a whole in situ and do not involve the separate exploitation of thepermitted illustrations or excerpts. Please view: STM Permissions Guidelines

20. **Warranties and Obligations:** LICENSOR further represents and warrants that, to thebest of its knowledge and belief, LICENSEE's contemplated use of the Content asrepresented to LICENSOR does not infringe any valid rights to any third party.

21. **Breach:** If LICENSEE fails to comply with any provisions of this agreement,LICENSOR may serve written notice of breach of LICENSEE and, unless such breachis fully cured within fifteen (15) days from the receipt of notice by LICENSEE,LICENSOR may thereupon, at its option, serve notice of cancellation on LICENSEE,whereupon this Agreement shall immediately terminate.

22. **Assignment:** License conveyed hereunder by the LICENSOR shall not be assigned orgranted in any manner conveyed to any third party by the LICENSEE without theconsent in writing to the LICENSOR.

23. **Governing Law:** The laws of The State of New York shall govern interpretation ofthis Agreement and all rights and liabilities arising hereunder.

24. **Unlawful:** If any provision of this Agreement shall be found unlawful or otherwiselegally unenforceable, all other conditions and provisions of this Agreement shallremain in full force and effect.

For Copyright Clearance Center / RightsLink Only:

     Service Description for Content Services: Subject to these terms of use, any termsset forth on the particular order, and payment of the applicable fee, you may make thefollowing uses of the ordered materials:**Content Rental:** You may access and view a single electronic copy of thematerials ordered for the time period designated at the time the order is placed.Access to the materials will be provided through a dedicated content viewer orother portal, and access will be discontinued upon expiration of the designatedtime period. An order for Content Rental does not include any rights to print,download, save, create additional copies, to distribute or to reuse in any way thefull text or parts of the materials.

     Content Purchase: You may access and download a single electronic copy ofthe materials ordered. Copies will be provided by email or by such other meansas publisher may make available from time to time. An order for ContentPurchase does not include any rights to create additional copies or to distributecopies of the materials

     Other Terms and Conditions:
     v1.18